IEEE Access
Multidisciplinary | Rapid Review | Open Access Journal

Received July 10, 2020, accepted August 22, 2020, date of publication September 7, 2020, date of current version September 21, 2020.

Digital Object Identifier 10.1109/ACCESS.2020.3022235

Evaluation of Charging Strategies for Valve Regulated Lead-Acid Battery

SANDHYA LAVETY, RITESH KUMAR KESHRI, (Senior Member, IEEE), AND MADHURI A. CHAUDHARI, (Senior Member, IEEE)
Visvesvaraya National Institute of Technology, Nagpur 440010, India

Corresponding author: Sandhya Lavety (sandhyalavety19@gmail.com)

This work was supported in part by the Young Faculty Research Fellow Scheme, Ministry of Electronics and Information Technology (MEITY), Government of India, under Grant MLA/MUM/GA/10(37)B, and in part by the Department of Science and Technology Scheme of the Science and Engineering Research Board (DST SERB) under Grant ECR002029/2016.

ABSTRACT The present paper considers the evaluation of temperature regulated and unregulated charging strategies to select the appropriate one to ensure extended battery life with reduced charging time. Temperature regulated pulse charging (TRPC) and temperature regulated reflex charging (TRRC) are compared with the Constant current–constant voltage (CC-CV) charging strategy. In the case of CC-CV charging temperature of the battery rises with the magnitude of the current being injected and cannot be regulated without any external cooling arrangement. Impact on the State of health (SOH) and the expected lifespan of the battery are considered as the parameters of evaluation. Temperature regulated strategies are implemented through a discrete electro-thermal model, which acts as a temperature estimator. The co-efficient of the estimators corresponds to the battery parameters such as internal resistance and thermal time constants, entropy, etc. Temperature regulation is ensured in the three identified sections of charge deposited vs magnitude of the injected current. Three sections are identified as sections where the injected current is not sufficient to raise the battery temperature to set limit or not and the level of charge submitted as compared to normal charging. Experimentation is carried with 12 V, 26 Ah Valve regulated lead-acid battery to justify that increase in temperature reference of regulation allows submission of higher charge for the same charging rate. It is demonstrated that TRPC results in a significant reduction ($\approx$60%) in charging time as compared to CC-CV and TRRC. For the same charging time as achieved with TRPC, TRPC results in almost double the expected life of operation and better SOH as compared to CC-CV and TRRC.

INDEX TERMS Discrete electro-thermal model, state of health, pulse charging strategy, reflex charging strategy, valve regulated lead acid battery.

I. INTRODUCTION

Electric vehicles (EVs) and plug-in electric vehicles are in high demand due to zero contribution to air pollution. Mainly Li-ion, Ni-metal hydride, Ni-Cd, and Lead-acid batteries are used as a power source in EVs. Among these batteries, Li-ion batteries are characterized with higher energy/power density, lightweight, and longer life as compared with the batteries of other chemistry. However, there are some constraints such as, requirement of Battery Management System (BMS), issue of overcharging, and regulation to full charging to keep per-cell voltage stress to a lower level [1], [2]. Whereas for the low-cost transportation solutions, still use of Valve Regulated Lead Acid (VRLA) battery is common for mass population due to its advantages over the constraints with Li-ion batteries. Longer charging time is a major concern in the adaption of EVs. This issue can be addressed through the concept of battery swapping or the fast charging of the batteries to reduce the charging wait time. Battery swapping requires a large infrastructural cost. Therefore, the emphasis is on charging strategies to reduce wait time. Batteries can be charged at a faster rate by injecting current at a higher rate than normal charging i.e. xC/10, where C is the capacity of the battery in Ah. In case of normal charging of the battery $x = 1$ and for faster charging $x > 1$. For example, if the battery capacity is 100Ah, then charging at 10A charging is normal and any injection more than this can be considered as faster charging. Normally, for a lead-acid

The associate editor coordinating the review of this manuscript and approving it for publication was Enamul Haque.

battery x is equal to one, whereas for the Li-ion battery the value of x can be greater than 10. If the current is injected at the rate above the normal rating of the battery, it not only can cause accelerated battery degradation, but also leads to other issues such as overcharging, temperature rises, and over-voltage. To resolve the above issues and ensure safe operation, a proper battery charging strategy should be implemented.

Several charging strategies have been discussed in the literature such as constant current (CC), constant voltage (CV), constant current-constant voltage (CC-CV), pulse charging, multi-step charging, and reflex charging [3]–[6]. Issues related to these charging strategies are high initial current, long charging time, corrosion of grids in plates, and higher temperature rise. In the case of a multi-step constant current (MSCC) charging strategy [4] a constant current is injected in steps to charge the battery, which reduces the charging time and improves the life cycle. The MSCC charging suppresses the sulfation of the negative plate and softening of positive plate material, which leads to the corrosion of grids in the positive plate. It also involves the memory effect caused by the shallow depth of discharge. The pulse and reflex charging strategies limit the problem of corrosion, sulfation, and dendrite formation which are responsible for the reduction in capacity and battery failure [7], [8]. Pulse charging strategy provides a short resting period after each charging pulse to reduce over potential problems whereas, in the case of reflex charging a short discharging pulse and rest period followed by charging pulse.

On the basis of the battery model, some of the researchers have optimized the charging time and comment on the effectiveness of the charging strategies. The battery model falls mainly into three categories: *i*) mathematical model, *ii*) electrical model, and *iii*) electrochemical model. The electrochemical model can predict run time and *v-i* performance by changing the chemical properties and provides microscopic parameter information [9]. However, it is time consuming and requires complex computational algorithms. A mathematical model is useful in system designs, adopts an empirical equation to predict system-level behaviors such as battery efficiency, run time, and capacity [10]. However, this model cannot offer any *v-i* information which is necessary for the simulation and optimization. Parameters of this model are obtained either by solving a system of equations or regression techniques of high computational complexity. The main disadvantage of a mathematical model is that the performance depends upon the algorithms used for the model extraction and varies from battery to battery. The electric equivalent circuit model can be easily simulated for the real-time behavior of the battery and information such as state of charge (SOC), terminal voltage, current, internal resistance, etc can be easily extracted. The electric equivalent circuit models are categorized as Thevenin's, impedance, and runtime-based model [11]. For reducing the charging time and to improve the battery performance several intelligent techniques have been proposed, such as the Ant colony [12], Gray prediction [13], Fuzzy [14], Neural Fuzzy [15], Trial-error method [16], and Taguchi method [17]. These intelligent techniques have reduced the charging time and increased the battery life to a great extent. However, battery thermal and health are not discussed in the above charging techniques.

Battery temperature not only affects the life but also reduces efficiency, energy, and battery capacity. In practice, battery operation and health are adversely affected by the low as well as the excess temperature [18]. Therefore, it is very important to consider the battery temperature variations while charging/discharging for the EV application [19].

Furthermore, some researchers considered an equivalent battery model to study the thermal behavior of a battery during the charging operation. An equivalent circuit model coupled with the thermal model is considered for analyzing the electrical and thermal behavior of the Li-ion battery [20]. The lumped thermal model is discussed [21] to simulate high precision temperature changes in the battery with the assumption of initial voltage values and by keeping the internal resistance constant. While both of these parameters affect battery current as well as voltage response. In [22], the thermal behavior of a Li-ion battery was predicted using a finite time approach. Hu *et al.* [23] proposes a dual objective-based optimal charging strategy for Li-ion which offers a tradeoff between charging time and energy loss.

Mentioned charging strategies with thermal models do not consider the situations with advanced control strategies such as sinusoidal current, multi-stage current injections, and temperature regulated controls for optimal charging. Such charging strategies for EV applications are discussed in the literature for efficient charging of the battery. In [24] a multi-stage fast charging technique is proposed for Li-ion batteries for electric vehicles. It reduces the charging time to 65%, extended the battery life, and improved the efficiency. However, in this charging technique battery health is not considered. AC ripple current to the charging current systematically results in new charging techniques i.e. pulse current charging and sinusoidal ripple current charging technique [25], [26]. An AC ripple current can be square or sinusoidal with a fixed frequency range from 100 to 1200Hz depending on the battery parameters. It reduces the charging time to 24% and lower the temperature rise to 50% as compared to the conventional CC-CV charging technique. Fine control with a quick response is however necessary to generate the precise current waveform and uses open-loop control based on a priori knowledge of cell parameters. Patnaik *et al.* [27] proposed a closed-loop constant temperature constant voltage charging technique which increases the charging speed to about 20% and reduces the temperature rise to 20%, through inexpensive computation as compared with optimization algorithms. The Predictive control for optimal charging [28] is implemented for the Li-ion battery, which improves the charging time and service life of the battery. In [29], genetic algorithm with specific objectives of charging time and temperature rise is presented for optimization. In [30], a closed-loop

optimal control was proposed to solve the optimum charging of a Li-ion battery with three objective functions namely energy loss, charging time, and thermal control by the CC-CV strategy. However, the variation in the internal resistance is not considered. Ouyang *et al.* [31] implements a distributed average tracking approach for optimal charging control of battery pack with the drawback of coupling characteristics. All the above strategies significantly optimize the charging time (CT), increase the efficiency, reduce losses, and control the temperature of the batteries by developing a proper battery model with different objectives function. However, the impact of charging strategies on battery health is not considered.

In addition, some of the researchers have studied the impact of optimal charging on battery health. Perez *et al.* [32] presents the optimal charging strategy by considering the electrical, thermal, and aging behavior of the Li-ion battery. However, model parameters which vary with aging are not updated. In [33], optimal multistage charging based on the electro-thermal-aging model is proposed for Li-ion battery. Partial swam optimization has been implemented with three objective CT, minimum battery aging, and balanced charging performance. However, the battery parameter with aging must be investigated. Liu *et al.* [34] proposed a multi-objective optimization considering economic costs of electrical energy loss and battery degradation based on the electro-thermal-aging model of a Li-ion battery. All these algorithms based on optimal charging strategy developed a proper battery model with different objective functions for optimal battery charging. However, most of the strategies are too complex to use in real-time monitoring.

Overall, it can be summarized that battery efficiency, health, and life mainly depend on the selected charging strategy. Therefore, it is necessary to develop a proper battery charging strategy which should control and monitor the battery temperature, improve battery health, and life. The electro-thermal and aging model serves as a temperature estimator during the charging process and plays an important part in an effective battery charging strategy. By considering all these important factors the present paper proposes the temperature regulated pulse charging (TRPC) and temperature regulated reflex charging (TRRC) strategies. It utilizes the discrete electro-thermal and aging model to study the electrical and thermal behavior of the VRLA battery and deposited charge as a function of charging current and temperature. Further, study the impact of proposed charging strategies on battery health through the aging model. The present case battery model and the charging strategy are not only applicable for a VRLA battery, but it is also applicable for other batteries such as Li-ion. This model is equally relevant to other charging strategies such as multi-step charging and can also be implemented for the battery pack.

Present work contributes to the current state of the art by *i*) utilizing a discrete electro-thermal and aging model to capture the electrical and thermal behavior of a VRLA battery through TRPC and TRRC strategies. By injecting higher current more than normal charging (C/10) for fast charging with set temperature reference and temperature band resulting in three operating sections: section 1, 2, and 3. Out of these sections, section 2 is considered as an effective operating region, since in this region charge deposited in the battery is more than normal charging, *ii*) It has demonstrated that with the upward shift in the temperature reference keeping temperature band fixed, faster charging can be achieved. *iii*) With the proposed TRPC strategy, it is possible to achieve up to 60% faster charging as compared to the normal C-rate (C/10). By proper cooling arrangement further, the charging time can be reduced, *iv)* Work is further extended through the aging model to study the impact of charging strategies on the battery health, *v*) It has demonstrated that for the same charging time and SOC level as achieved with TRPC strategy, the CC-CV results in higher operating temperature 53°C resulting in a reduction in the expected life around 10 months and a relatively higher drop in the state of health. In the case of TRRC strategy at the same time and SOC level, the battery temperature is operated within the temperature band (42-45.2°C) with 3.3(C/10) with an expected life of 16 months. Whereas in the case of TRPC strategy (2.65C/10) the battery temperature is within the band of (36-39°C) and extending the life of the battery to 24 months, and *vi)* It has demonstrated that the TRPC strategy apart from reducing the charging time, it also improves the battery health and life.

The Present paper is organized as: Section-II elaborates the discrete electro-thermal and aging model of the VRLA battery. Charging strategies are discussed in section-III. Section-IV describes proposed charging strategies. Experimental procedures are carried out in section-V. Results and discussion are presented in section-VI. The final conclusions are drawn in Section VII.

II. DISCRETE ELECTRO-THERMAL AND AGING MODEL

The electro-thermal and aging model of a battery consists of an equivalent electric model, thermal model, and aging model of the battery. Fig.1 shows the block diagram representation of a battery model. With the information of sensed battery current and terminal voltage, the equivalent electric model determines the state of charge (SOC), open-circuit voltage (V_{OC}), and internal resistance of the battery $R_{int,}$ where $R_{int} = R_{c1} + R_c$. The thermal model uses this information together with the entropy of the battery material, ambient temperature, and internal resistance to estimate the battery temperature (T_{bat}). R_{int} also depends upon the battery temperature, so the equivalent electric model uses the information of T_{bat} to update the value of R_{int}. With the estimated battery temperature and sensed battery current the aging model estimates the state of health of the battery. However, the battery parameter with aging has to be investigated.

A. EQUIVALENT ELECTRIC CIRCUIT MODEL

An equivalent electric circuit model of a battery is shown in Fig.2. Where R_c is the internal resistance of the battery during charging, R_d internal resistance of the battery during

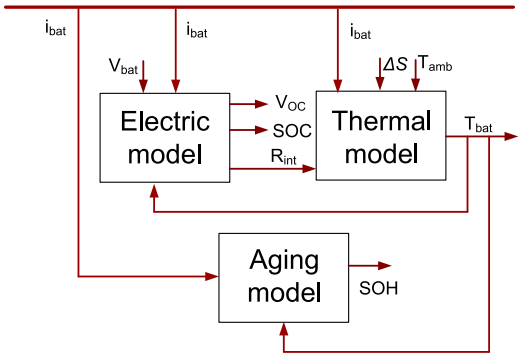

FIGURE 1. Block diagram representation of a battery model.

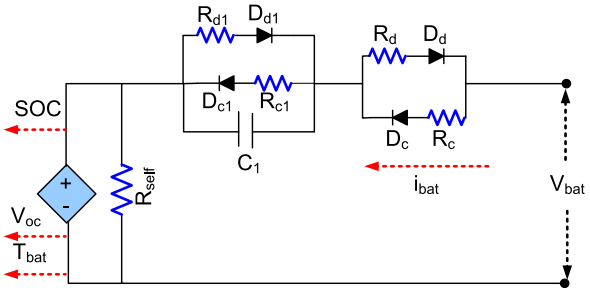

FIGURE 2. Equivalent electric circuit model of a battery.

discharging, R_{c1} is over voltage resistance of the battery during charging, R_{d1} is over voltage resistance during discharging, C_1 is over voltage capacitor, and R_{self} is self-discharging resistance. The capacitance 'C_1' of the $R_{c1}C_1$ pair of the battery model is considered as relatively constant over a battery lifetime. Since it depend on the mass of the rolled electrode assembly, casing, and thermal properties of the material [35], [36].

The electric model determines the battery terminal voltage, SOC, open-circuit voltage (V_{oc}), and internal parameters of the battery during charging/discharging.

The SOC can be calculated by current integration method [37].

$$SOC\,(t) = SOC(0) + \frac{\int i_{bat}dt}{Ah_o} \tag{1}$$

where initial SOC is *SOC(0)* and Ah_o is the specified battery capacity for the present case it is 26Ah. SOC in each step should be added to the previous value.

This value is further utilized to calculate the open-circuit voltage of the battery by means of curve fitting method through information provided by manufacturer datasheet and is given as,

$$V_{oc}\,(SOC) = \alpha \times SOC + \beta \tag{2}$$

where, constant $\alpha = 1.4$ and $\beta = 11.9$

B. THERMAL MODEL

The heat generated inside the battery depends on the battery chemistry, ambient temperature, and battery types. The total heat generated is mainly due to heat generated by joule and entropy heat. Total heat generated H_{gen} inside the battery is given by,

$$H_{gen} = H_{joule} + H_{entropy} \tag{3}$$

where, H_{joule} is heat generation and $H_{entropy}$ is entropy heat.

Heat generation due to joule is given by,

$$H_{joule} = \int i_{bat}^2 . R_{int} dt \tag{4}$$

where, total internal resistance during charging is $R_{int} = R_{c1} + R_c$

The energy equation used to calculate the battery temperature is given by [38],

$$m \cdot C_p \frac{dT_{bat}}{dt} = i_{bat}^2 \mathrm{R_{int}}(n) + T_{bat}\frac{\Delta S i_{bat}}{eF} - \mathrm{A}\left\{T_{bat}\,(n) - T_{amb}\right\} h \tag{5}$$

where, m is the mass of the battery, C_p is the specific heat capacity, e is the number of electrons, F is Faraday's constant for the battery, and T_{amb} is the ambient temperature. First term in (5) is heat due to joule, second term is entropy heat, and the last term is heat transferred to surrounding.

As per Newton's law of cooling dynamics of the battery temperature during charging is given by,

$$\frac{dT_{bat}}{dt} = -\lambda(T_{bat} - T_{amb}) \tag{6}$$

Equation (4) is in continuous time domain and for the use as estimator in micro-controller discretization of it is required.

$$\frac{H_{gen}\,(n+1) - H_{gen}\,(n)}{t_s} = i_{bat}^2\,(\mathrm{n})\,\mathrm{R_{int}(n)} \tag{7}$$

$$T_{rise}\,(n+1) = T_{rise}\,(n) + \frac{R_{int}(n)t_s}{mC_p} i_{bat}^2(n) \tag{8}$$

$$T_{rise}\,(n) + T_{amb} = T_{bat}\,(n) \tag{9}$$

Substitution from (9) to (8) further results in estimated battery temperature

$$T_{bat}\,(n+1) = T_{bat}\,(n) + \frac{R_{int}(n)t_s}{mC_p} i_{bat}^2\,(n) - \{T_{bat}\,(n) - T_{amb}\}\,(\lambda t_s) \tag{10}$$

where, rate of cooling λ is given by,

$$\lambda = \frac{Ah}{C_p m} \tag{11}$$

From equation (5) and (10) discrete electro-thermal model is given by

$$\begin{aligned} &T_{bat}\,(n+1) \\ &= T_{bat}(n) + \frac{R_{int}(n)t_s}{mC_p} i_{bat}^2\,(n) \\ &\quad + T_{bat}\,(n)\left\{\frac{\Delta S}{mC_p eF} t_s\right\} i_{bat}(n) - \lambda t_s\,\{T_{bat}\,(n) - T_{amb}\} \end{aligned} \tag{12}$$

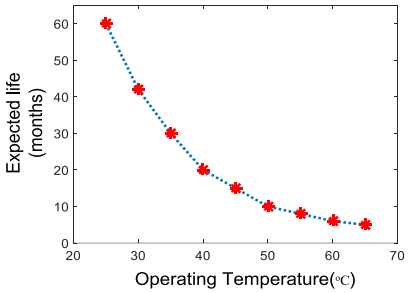

FIGURE 3. Impact of operating temperature on the expected life of a battery [41].

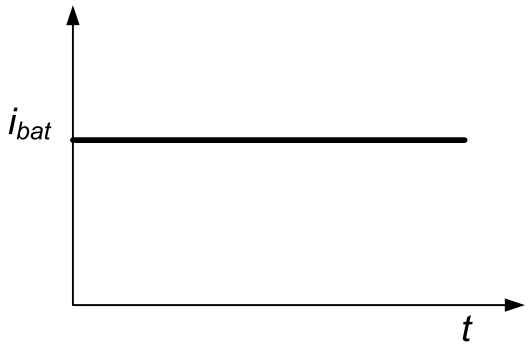

FIGURE 4. Constant current strategy.

In equation (12) the second term related with heat due to joule, third term is entropy heat and the last term is related to heat dissipation. where, mass of the battery is $m = 9.6kg$, specific heat capacity is $C_p = 0.22Wkg/K$, ambient temperature is $T_{amb} = 25°C$, area of the battery is $A = 0.062m^2$, Heat transfer coefficient is $h = 100W/m^2K$, t_s is the sampling time, rate of cooling is $\lambda = 0.003/sec$, change in entropy $\Delta S = eF(\partial E_{eq}/\partial T)$ and $\partial E_{eq}/\partial T$ is the temperature coefficient of a VRLA battery. These specifications are taken from the battery datasheet and referred standard textbook [39], [40].

In equation (12), term $\{(\Delta S/(mC_peF)\}t_s$ ($\approx -0.157 \times 10^{-9}$) is negligible, so it is neglected. Thus, the discrete model can further be simplified to

$$T_{bat}(n+1) = T_{bat}(n) + \frac{R_{int}(n)t_s}{mC_p} i_{bat}^2(n) - \lambda t_s \{T_{bat}(n) - T_{amb}\} \quad (13)$$

Temperature is the key parameter and it should be considered during the development of the optimal charging strategy. If the battery is injected with a higher C-rate, it leads to increase in the battery temperature, affects the battery life, and even causes the thermal runaway. The impact of operating temperature on the expected life of the battery, which reduces with the increase in operating temperature, is shown in Fig.3 [41]. Therefore, while increasing the speed of the charging, regulation of temperature within the permissible limit must be ensured.

C. AGING MODEL

Battery health is an important issue that should be addressed during the optimal battery charging strategy. The aging process of a lead-acid battery is mainly due to the anodic corrosion, irreversible formation of lead sulphate in the active mass, loss of water, and short circuit. The state of health (SOH) is an estimator, which supplies the information of degradation to the battery and whether the battery should be replaced or not. As per the Arrhenius equation, the expected lifetime of the battery at operating temperature T_L is given by,

$$t_{life} = \gamma \times exp\left(-E_a/RT_L\right) \quad (14)$$

where, E_a is the activation energy, R is the gas constant, and γ is the pre-exponential factor, and are equal to 10500 cal/mol, 1.987 cal/mole/kelvin, and 1.5×10^4 respectively for a VRLA battery.

The battery life is model by,

$$\Delta \mathrm{Ah}(\mathrm{t_{serv}}) = \gamma \cdot \exp\left(-\mathrm{E}/\mathrm{RT_L}\right) \cdot \mathrm{t_{serv}^z} \quad (15)$$

This equation (15) follows simple laws based on power of time and Arrhenius kinetics. Where, z is the exponent of time. For simple diffusion control z = 0.5 [42]. In this case, instead of using time used Ah throughput as a parameter for the age modeling of a battery.

Battery capacity with service time is given by,

$$Ah\,(\mathrm{t_{serv}}) = \mathrm{Ah_0} - \Delta Ah\,(t_{serv}) \quad (16)$$

where, $\Delta Ah\,(t_{serv})$ is the drop in the capacity of the battery after the operation/service period of t_{serv} since the first use. Ah_0 is the specified capacity of the battery. Further if the charging is being carried out for time duration $t_2 - t_1$, and is equivalent to N number of (charge/discharge cycle) then the battery state of health is given by [32],

$$\mathrm{SOH}\,(t_{serv}) = \mathrm{SOH_0} - \frac{\int_{t1}^{t2} i_{\mathrm{bat}}\mathrm{dt}}{2NAh_0} \quad (17)$$

For a fresh battery $SOH_0 = 1$. Where, N is the number of cycles which is the function of temperature.

In the present discussion aging model is used to evaluate the impact of charging strategies on the battery health.

III. CHARGING STRATEGIES

A. CONSTANT CURRENT (CC) STRATEGY

One of the most common method of battery charging is the constant current charging. Depending upon C-rate of the battery, a constant current is supplied to it. The constant current strategy is shown in Fig.4.

It normally takes 8 to 10 *hrs* to charge a VRLA (C/10) battery, whereas in the case of Li-ion (1C) it charges within one hour. However, in this method, if the current is supplied beyond the C-rate of the battery the temperature of the battery rises and the average life of the battery is decreased due to overcharging and gassing problems. Hence, this method is not suitable for the fast charging of the battery.

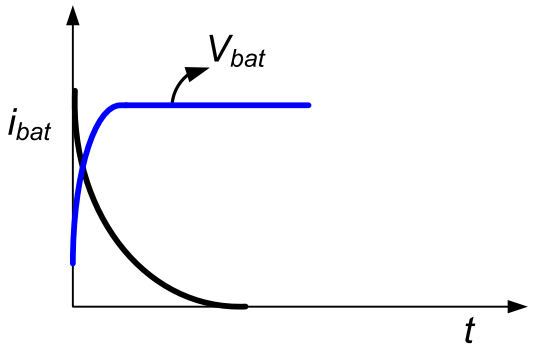

FIGURE 5. Constant voltage strategy.

B. CONSTANT VOLTAGE (CV) STRATEGY

A constant voltage strategy is shown in Fig.5. In this strategy, a constant voltage is maintained throughout the operation. While maintaining constant voltage, the initial current becomes very high. A high initial current result in high temperature rises and hence the life of the battery is affected. This form of charging method however needs to have a very stable output voltage. This charging strategy is not practical because of the requirement of high current capacity that results in a high cost.

C. CONSTANT CURRENT-CONSTANT VOLTAGE (CC-CV) STRATEGY

Another charging strategy is the constant current constant voltage (CC-CV) charging strategy as shown in Fig.6. It is the most widely used strategy for Li-ion batteries. In this method, the constant current is supplied to the battery and when the terminal voltage reaches the maximum limit the control is governed by a constant voltage charging. Later, the charging current reduces to a threshold value. However, this strategy requires a long charging time if normal C-rate is supplied to the battery. And, if the higher current (more than C-rate) is supplied continuously, it leads to the temperature rise and even causes thermal runaway. Chen and Lai [43] proposed a new digital controlled charger technique for CC-CV operation without the need for current control by limiting the duty cycle of a charger and thus reducing the overall cost of A/D converters and current sensors. In [27] closed-loop constant temperature constant voltage technique is proposed for Li-ion batteries. PID controller is employed with feed-forward aid. It is computational inexpensive as compared to optimization algorithms. However, in CC-CV strategy the current rate is still a big issue since the higher current leads to the temperature rise and lower current increase the charging time.

D. PULSE CHARGING STRATEGY

The pulse charging strategy is shown in Fig.7. In the case of a VRLA battery, during the charging cations and anions formed in electrolyte form a double layer which causes an over potential and affects the efficiency of the battery. To reduce this over potential the pulse charging strategy allows for a

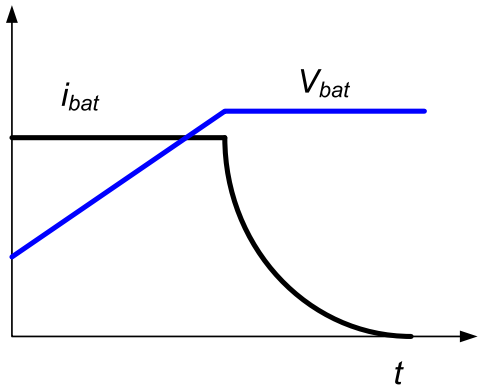

FIGURE 6. Constant current constant voltage strategy.

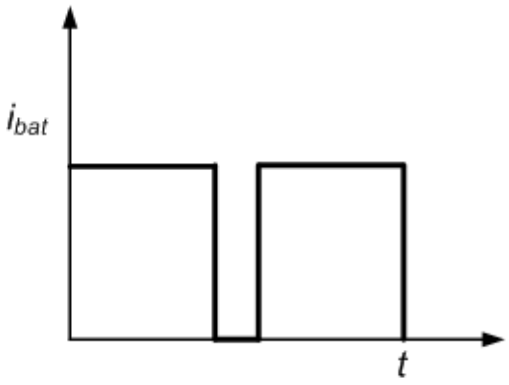

FIGURE 7. Pulse charging strategy.

short resting period after each charging pulse. Furthermore, this strategy also reduces sulfation, which is the main reason for the battery failure.

In literature it has justified the extension in the life of batteries by suppressing the problem of sulfation for example, *i*) addition of Grapheme (Gr) to the negative active material improves the life cycle from 7078 to 17157 (by 140%) [44] and *ii*) 3D reduced grapheme oxide material extended the life cycle from 8142 to 26425 (more than 224%) [45]. In practice, VRLA batteries should be charged at a normal rate i.e. xC/10 ($x = 1$) resulting in a charging time up to 10hrs. Any increase in the C-rate results in faster charging at the cost of overcharging and overheating. The overheating problem can also lead to thermal runaway. This issue of overcharging is addressed through the adoption of intermittent charging [46], Quick charge with frequency technique [47], synergetic control [48], and rapid charging with energy recovery [49]. In all the above strategies, different cases of pulse charging have been adopted to overcome the problem of overcharging. Whether it is a pulse or reflex charging, to solve the problem of overheating in any situation, the pulse width should be just that much for which the temperature rise does not exceed the permissible limit. To achieve the regulation of charging pulse-width information of battery temperature is required and can be obtained through the sensors [50] or from electric/electro-thermal model of the battery.

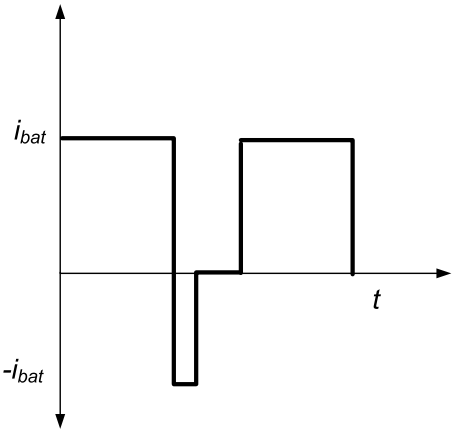

FIGURE 8. Reflex charging strategy.

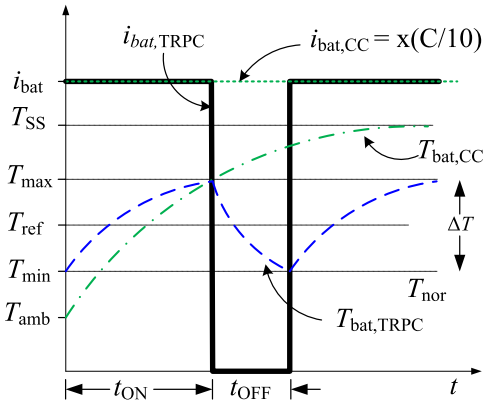

FIGURE 9. Operational waveform of a temperature regulated pulse charging.

E. REFLEX CHARGING STRATEGY

This is another method to charge the battery. It consists of a charging pulse, discharging pulse, and resting period. The reflex charging strategy is shown in Fig.8. Crystalline formation and dendrites growth both are stopped through the reflex charging strategy. Dendrites are particles formed on the surface of the electrode during the charging process which can cause a short circuit. Overall, several charge and discharge cycles particularly when the battery is cycled at a fast rate, microscopic lithium fibers called dendrites sprout from the surface of the lithium electrode and spread through the electrolyte until they reach to the other electrode. The most common way to discharge the battery during a negative pulse is through the resistive load. That causes excessive heat dissipation and reduces efficiency. Non-dissipation during a negative pulse is presented in [49]. However, the control is complicated with two switches. A novel circuit with one switch is presented by [51] to generate a pulse for battery charging. However, it requires an extra energy tank to store negative pulse energy temporarily and then returns to the battery during a charging process. This problem is solved by the energy recovery function for a bidirectional converter in which the negative pulse energy of the current profile reduces the dissipation of the battery by using a single capacitor bus [8]. However, in all the above charging strategies optimal charging, battery health, thermal, and life are not considered.

IV. PROPOSED CHARGING STRATEGIES

In this present work, a temperature regulated pulse and reflex charging strategies are proposed to reduce the charging time and to ensure improvement in battery health and life. A comparative analysis is done that helps to find a suitable charging strategy for the fast charging of EVs with the same charging time and SOC level to improve battery life and health.

The operational waveform of temperature regulated pulse charging strategy is shown in Fig.9. If higher current more than the normal charging current (xC/10) is injected in the battery, where x >1 temperature increases from ambient (T_{amb}) to steady-state temperature (T_{SS}). The green dash line represents a constant current temperature rise. For fast charging higher value of 'x' is injected into the battery, under such a condition battery temperature (T_{bat}) rises above the maximum limit and even can cause thermal runaway. To ensure temperature regulation, the hysteresis band has set two limits maximum (T_{max}) and minimum (T_{min}) temperature limit in related to variable temperature reference (T_{ref}) and fixed temperature band $\Delta T = 3°$C. When T_{bat} reaches the maximum limit T_{max}, $i_{bat,TRPC}$ set to zero and T_{bat} starts reducing to a minimum set limit. As soon as the $T_{bat} = T_{min}$ again $i_{bat,TRPC}$ is supplied to the battery and this cycle repeats until the battery is charged up to 95% SOC. This strategy results in a TRPC strategy. The blue dash line reflects the temperature regulation for the pulse charging strategy. The operational waveform of a TRRC strategy is shown in Fig.10. For this strategy, three limits are set for control operation T_{max}, $T_{min,}$ and T_{dis}. For fast charging when higher current is injected into the battery, the battery temperature increases and when it reaches to T_{max} the battery supply power to the input capacitor until $T_{bat} = T_{dis}$. As the temperature of the battery increases to T_{dis}, $i_{bat,TRRC}$ set to zero, and T_{bat} starts reducing. Once the $T_{bat} = T_{min}$ again battery starts charging by $i_{bat,TRRC}$. The same process is repeated until the battery is charged up to 95% of SOC. The red dash line represents the temperature regulation of the reflex charging strategy. For both the strategies ΔT is kept constant (3°C) and T_{ref} is varied and studied the impact on the total charge submitted within a fixed interval of time.

V. EXPERIMENTAL PROCEDURE

A. CHARGING CIRCUIT FOR PULSE AND REFLEX CHARGING STRATEGIES

The charging circuit for the pulse charging strategy is shown in Fig.11 and the charging circuit for the reflex charging is shown in Fig.12. It consists of an AC grid, AC-DC uncontrolled rectifier with filter capacitor C_{ref}, DC converter, and a VRLA battery of 12 volts 26Ah rating. Note that for CC, CV, CC-CV, and pulse charging buck converter is used to

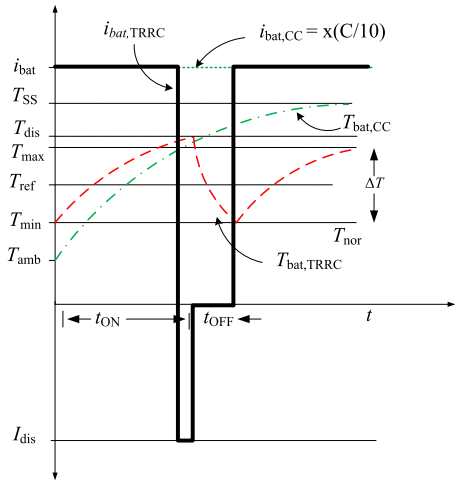

FIGURE 10. Operational waveform of a temperature regulated reflex charging.

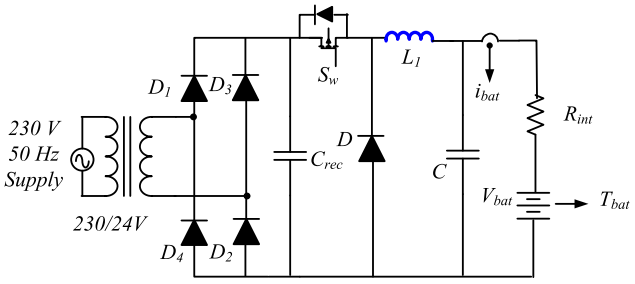

FIGURE 11. The charging circuit for the pulse charging strategy.

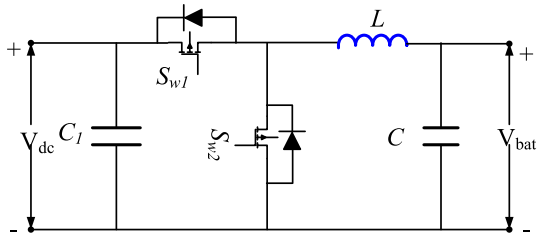

FIGURE 12. The charging circuit for the reflex charging strategy.

verify the results and the bi-directional converter is used for reflex charging strategy. For buck converter single power MOSFET S_w is used with anti-parallel diode, inductor L, and a capacitor C. For reflex charging bidirectional converter consists of two power MOSFETs Sw_1 and Sw_2 with anti-parallel diodes D_1 and D_2.

B. EXPERIMENTAL SET-UP

The experimental setup for a battery charger circuit is shown in Fig.13. This charging circuit consists of an uncontrolled rectifier, converter, fan, and fuses for protection. The control action is carried out through the DSP TMS320F28335 microcontroller. Two types of sensors are used for this test procedure such as voltage sensor LV 25-P and current sensor LA-5P. In the present work, the temperature of the battery is estimated by the means of the thermal model as given in

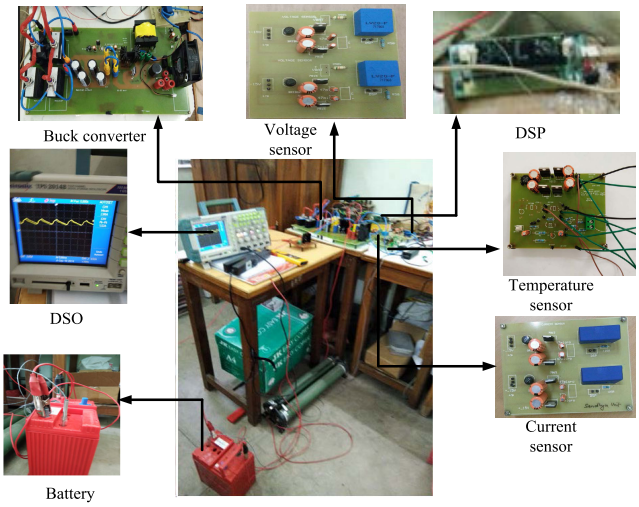

FIGURE 13. Experimental setup for a battery charger circuit.

equation (13). Control has been implemented through DSP. The battery temperature is updated for each sampling period with details of the sensed battery current at the sensed battery voltage. The sensed current is converted into an equivalent voltage within the acceptable limit of analog to digital (ADC) input voltage level to micro-controller. Which is further processed as per the bit (32 bit) size of the address for an example in case of TMS320F28335 processor for ADC output is 0 to 4096 for the input of 0 to 3.3V. The temperature measurement circuit using R_{RTD} is used to cross verify the electro-thermal and aging model. Specifications of the battery charging circuit are indexed in Table 1.

TABLE 1. Specification of battery charging circuit.

Symbol	Quantity	Value
L_1	inductor	45mH
C	capacitor	390 µF
P	power	150W
Swf	switching frequency	20kHz
V_{out}	output voltage	12 volts
V_{in}	input voltage	24 volts
LV25-P	voltage sensor	$100V_{max}$
LA55P	current sensor	$50\ I_{max}$

C. CONTROL STRATEGY FOR TEMPERATURE REGULATED CHARGING

A block diagram of the control strategy of temperature regulated pulse charging is shown in Fig.14a. For control operation, it consists of two main parts. The first one is the current generator and the second one is the controller. The charging strategy works according to these two's decisions. *a*) Current generator: The current generator receives two inputs, i.e. battery current (i_{bat}) and battery temperature (T_{bat}). For temperature regulated pulse charging strategy, the battery temperature is divided into two modes. In the first mode, T_{bat} lies between maximum temperature (T_{max}) and minimum temperature (T_{min}). During this mode constant current is injected into the battery. In the second mode, if $T_{bat} \geq T_{max}$

TABLE 2. Comparative evaluation of different charging strategies.

Charging strategy	Maximum temperature	Total charge deposited in one hour (A·s/coulomb)	Charging current magnitude *x*(C/10)	Total charging time(hrs)	SOH Decay	Life
CC-CV	53°C	15000	2.3(C/10)	4.25	more	10 months
TRPC	36-39°C	22000	2.65(C/10)	4.25	less	24 months
TRRC	42-45.2°C	22300	3.3(C/10)	4.25	less	16 months

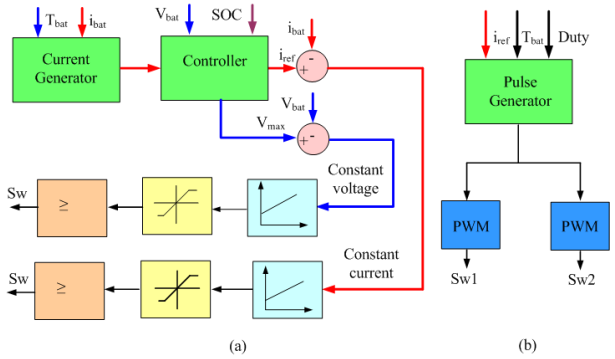

FIGURE 14. Block diagram of control strategy of temperature regulated pulse and reflex charging strategies.

the reference current is set to zero until T_{bat} is less than T_{min}. *b*) Controller: Three inputs are given to the controller i.e. reference current, SOC, and terminal voltage. The controller decides whether the charging strategy to operate in constant current mode or in constant voltage mode. If the SOC reaches a pre-set value, then the constant voltage mode started, otherwise constant current mode will operate. The temperature regulated reflex charging strategy consists of three main parts i.e. controller, current generator, and pulse generator. Fig.14 shows the block diagram of the control strategy for temperature regulated reflex charging strategy. For reflex charging strategy the T_{bat} is divided into three modes. In the first mode, the T_{bat} lies between T_{min} and the maximum limit of temperature during charging (T_{max}). If the battery temperature lies in between these, a constant current is injected into the battery. In the second mode, T_{bat} lies between T_{max} and maximum limit of temperature during discharging (T_{dis}). At this mode, a battery supplies the current to the input capacitor. In the third mode, when T_{bat} becomes more than T_{dis}, the battery stops charging and the same cycle is repeated until the battery is charged up to 95% of SOC. The third main part of the control strategy for reflex charging is a pulse generator. It has three inputs i.e. reference current, battery temperature, and duty ratio. Based on reference current and T_{bat}, a pulse is generated for two switches. Switch S_{w1} will operate when power is supplied to a battery during charging and during the discharging condition, switch S_{w2} will operate and power is supplied from battery to the input capacitor. The control strategy for the temperature regulated pulse and reflex charging is explained through a flowchart as shown in Fig.15.

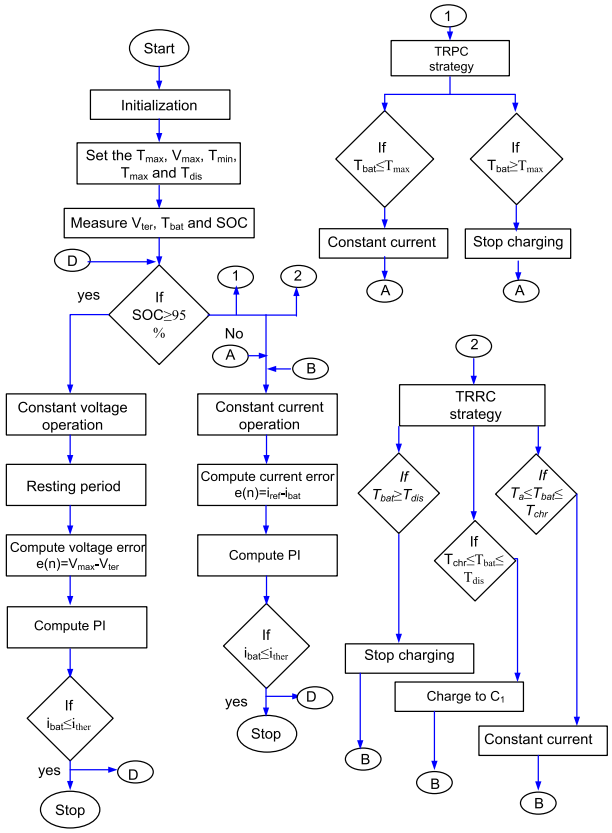

FIGURE 15. Flow chart of a control strategy.

VI. RESULTS AND DISCUSSION

A. EFFECT ON CHARGE DEPOSITED WITH CONSTANT TEMPERATURE REFERENCE

Effect on charge deposited with constant temperature reference for the temperature regulated pulse and reflex charging shown in Fig.16. Where '*x*' is the multiplying factor and is equal to the ratio of charging current to the normal current (C/10). The graph is divided into three sections i.e. section 1, 2, and 3.

Section 1: In this section, the level of charging current is not high, so the battery temperature does not exceed the maximum limit of that band. As a result, in this section, a constant current is supplied to the battery. The total charge deposited into the battery is considered for one-hour duration. Under normal charging (C/10) the total charge deposited within the battery is 9360 coulomb or As.

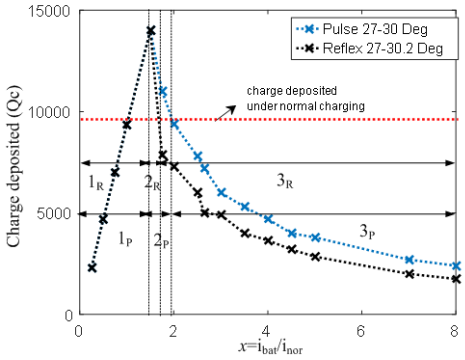

FIGURE 16. Effect on charge deposited with constant T_{ref} for temperature regulated pulse and reflex charging.

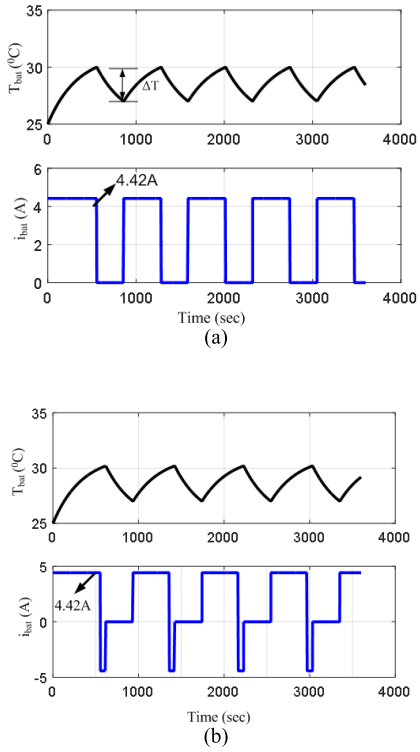

FIGURE 17. (a). The temperature regulated pulse charging strategy for section 2. (b). The temperature regulated reflex charging strategy for section 2.

Section 2: In this section, the level of charging current is such that a pulse and reflex charging mechanism occurs. Here, as the battery temperature reaches T_{max}, the current set to zero until T_{bat} becomes equal to T_{min}. If $T_{bat} = T_{min}$, a constant current will be applied again. It is the effective region of operation, where the temperature is under control and fast charging of a battery is possible.

Fig.17 (a) and (b) shows the temperature regulated pulse and reflex charging strategies for section 2 with 4.42A. The present analysis was carried out for 3600 seconds for TRPC strategy with, $T_{ref} = 28.5°C$, $T_{max} = 30°C$, and $T_{min} = 27°C$ and for TRRC strategy with $T_{ref} = 28.5°C$, $T_{max} = 30°C$, $T_{dis} = 30.2°C$, and $T_{min} = 27°C$.

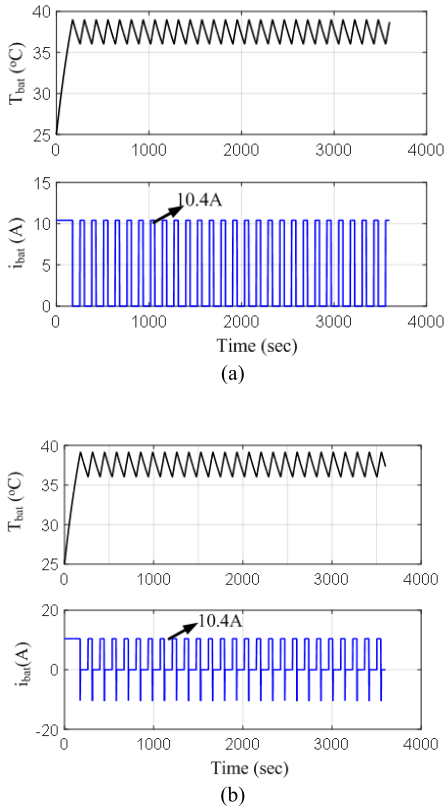

FIGURE 18. (a). The temperature regulated pulse charging strategy for section 3. (b). The temperature regulated reflex charging strategy for section 3.

Section 3: This is the last section, where the temperature is regulated but the charge deposited into the battery is lower than in section 2. Since in this section level of charging current is very high, ON time pulse is less than OFF time. Fig.18 (a) and (b) shows the temperature regulated pulse and reflex charging strategies for section 3. 1_R, 2_R, and 3_R are the notations defined for sections for reflex charging strategy and similarly notations 1_P, 2_P, and 3_P are the sections defined for pulse charging strategy.

B. EFFECT ON CHARGE DEPOSITED WITH VARYING CURRENT AND TEMPERATURE REFERENCE

The total charge deposited into the battery with varying temperature reference and current for TRPC and TRRC strategies are shown in Fig.19. Two temperature references 28.5°C (notation for pulse charging is 1_P, 2_P, 3_P and for reflex is 1_R, 2_R, 3_R) and 37.5°C (notation for pulse charging is 1_{PF}, 2_{PF}, 3_{PF} and for reflex is 1_{RF}, 2_{RF}, 3_{RF}) are used to demonstrate the effect of charge deposited to the battery for the same charging C-rate. Set temperature reference is an average of the maximum and the minimum value of the temperature band, and are 27°C and 30°C respectively for temperature reference 28.5°C and similarly 36°C and 39°C for 37.5°C. For both cases a fixed temperature band of 3°C is considered. In any case, the maximum value of the temperature for a particular reference can never be higher than the temperature

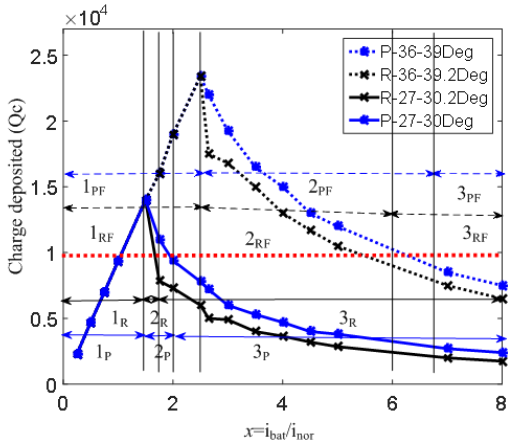

FIGURE 19. Total charge deposited with varying temperature reference and current for TRPC and TRRC strategy.

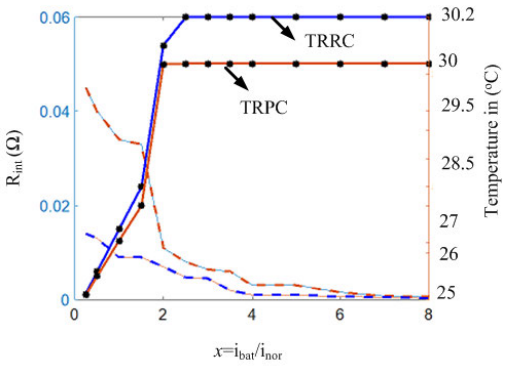

FIGURE 20. Effect of battery temperature and i_{bat} on internal resistance for TRPC and TRRC strategy with 28.5°C T_{ref}.

specified as per the datasheet of the battery, which is 50°C in the present case. The reason for selecting temperature reference 28.5°C and 37.5°C is to keep the set temperature limits higher than the ambient temperature 25°C. In addition, it has been observed in Fig. 19 that with the increase in temperature reference, Sections (1, 2, and 3) of operation shifts upward resulting in the increase in the submission of charge into the battery at the same C-rate. The logic behind considering the fixed temperature band is the advantage of a higher magnitude of the deposited charge as compared to the case of fixed temperature reference and variable temperature band. It can also be concluded that the increase in temperature reference results in the faster charging of the battery because of the increase in the pulse width of the charging current. From the graph, it can be observed that maximum charge deposited is more in the case of the TRPC strategy than the TRRC strategy. In temperature regulated reflex charging strategy, a positive pulse is followed by a negative pulse with a resting period whereas, during a negative pulse, a battery supplies power to the input capacitor. So, it is obvious that the charge deposited during TRRC is lower than the TRPC strategy for same temperature band.

C. EFFECT OF TEMPERATURE ON INTERNAL RESISTANCE OF A BATTERY

This is the essential parameter that should be taken into account during the charging strategy. It is considered as constant in some cases but in actual practice, it is not constant it varies with the battery temperature, current, and time. This sub-section discusses the deviation in the internal resistance (R_{int}) with the battery temperature (T_{bat}) and battery current (i_{bat}). According to the electro-thermal model, it is updated during the charging strategy. The effect of T_{bat} and i_{bat} on R_{int} for TRPC and TRRC strategies with temperature reference of 28.5°C is shown in Fig. 20. From the graph, it is clear that R_{int} varies during the lower magnitude of the charging current, but it remains almost constant for higher C-rate.

Equivalent internal resistance during charging is given by,

$$R_{int}(n) = \frac{V_{bat}(n) - V_{oc}(n)}{i_{bat}(n)} \tag{18}$$

where, R_{int} is the total of internal resistance of the battery during charging $R_{int} = R_c + R_{c1}$, V_{bat} is the terminal voltage, V_{oc} is open-circuit voltage, and i_{bat} is the battery current. From the graph, it is clear that the total internal resistance is influenced by both i_{bat} and T_{bat} and is given as,

$$R_{int} = f\,(i_{bat}) \cdot g\,(T_{bat}) \tag{19}$$

The dependency of R_{int} on battery current is fitted by exponential function and is given as,

$$f\,(i_{bat}) = a_{rint} i_{bat}^{brint} \tag{20}$$

The dependency of R_{int} on battery temperature is fitted by polynomial function and is given as,

$$g\,(T_{bat}) = c_{rint} T_{bat} + d_{rint} \tag{21}$$

where, $a_{rint} = 0.0217$, $b_{rint} = -0.6344$, $C_{rint} = -0.008351$ and $d_{rint} = 0.2546$.

D. EVALUATION OF CHARGING STRATEGIES

The CC charging of a VRLA battery with normal C/10 charging is shown in Fig.21. In CC charging a constant current is injected in the battery and it takes 10 hours to charge the VRLA battery. It is seen from the experimental result that when normal current is supplied to the battery, the T_{bat} rises from ambient and settles down to the steady-state temperature (27.5° C). Fig. 22 shows the charging profile for CC-CV with C/10 charging current. In this strategy, the constant current is injected into the battery resulting in the increased terminal voltage. When the terminal voltage reaches the pre-set value, control is switched to constant voltage charging. During constant voltage charging, voltage is maintained constant and current starts reducing to zero. The total time taken to charge the battery for this case is 9 hours. The operational waveform of the TRPC strategy with 1.7C/10 is shown in Fig. 23. An experimental result of a single pulse of the TRPC strategy is shown in the graph. It is proven that when a constant current is supplied to the battery, T_{bat} increases to the maximum limit

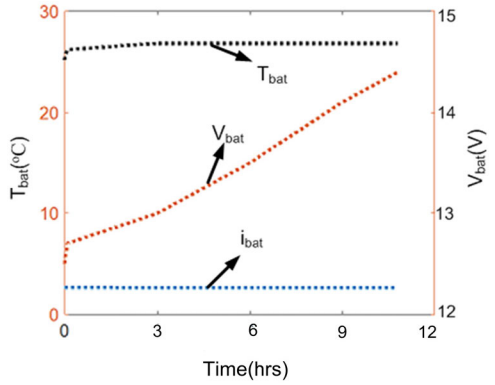

FIGURE 21. The charging profile of CC charging for a VRLA battery with C/10 charging.

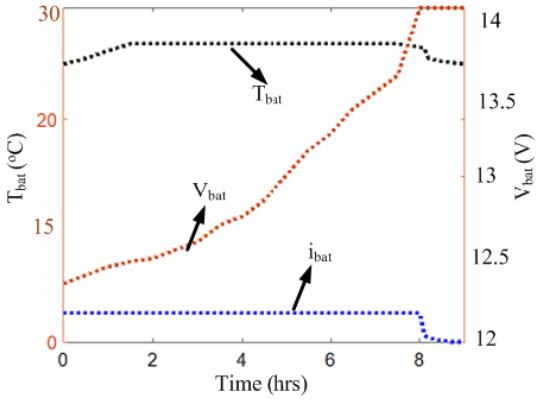

FIGURE 22. The charging profile for CC-CV charging with C/10 charging.

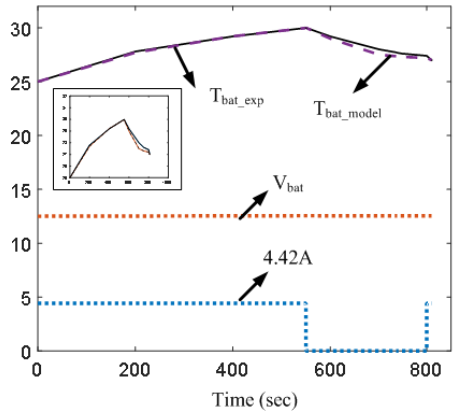

FIGURE 23. Operational waveform of the TRPC strategy with 1.7C/10 current.

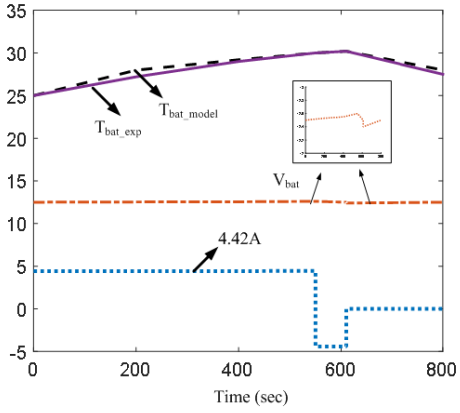

FIGURE 24. Operational waveform of the TRRC strategy with 1.7C/10 current.

of the hysteresis band. When $T_{bat} \geq T_{max}$ then current set to zero and T_{bat} start reducing to the minimum limit. As soon as the $T_{bat} = T_{min}$ again $i_{bat,TRPC}$ is supplied to the battery. The operational waveform of a TRRC strategy with 1.7C/10 is shown in Fig. 24. It is verified that the model result in approximately matches the experimental result. From the graph, it is clear the V_{bat} decreases during the negative pulse, and its value starts to increase for the resting period and becomes a steady state. Its value again begins to increase for next charging pulse.

E. EVALUATION OF BATTERY HEALTH AND LIFE FOR SAME CHARGING TIME AND SOC LEVEL

The SOH decay for the CC-CV, TRPC with T_{ref} (37.5°C), and TRRC with T_{ref} (43.5°C) strategies based on equation (17) is shown in Fig. 25. It is verified that SOH decay for CC-CV strategy is more than TRPC and TRRC strategy. The SOH decay is less for the TRRC strategy since in this charging strategy the battery is charged and discharged for each charging pulse. So, battery health deteriorates less in the case of the reflex charging strategy. Fig. 26 shows the variation in charging current and operating temperature for CC-CV, TRPC, and TRRC strategies. It is clear from the graph that

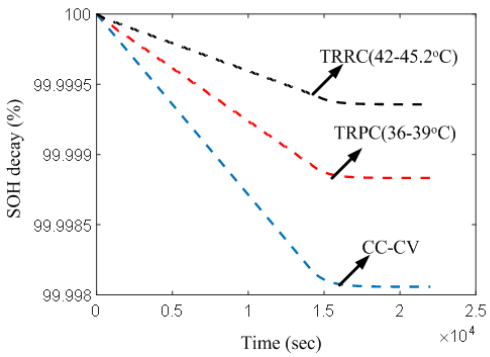

FIGURE 25. Shows the SOH decay for the CC-CV, TRPC, and TRRC strategies on the basis of (17).

for CC-CV charging during CC mode constant current is injected into the battery. The T_{bat} rises from ambient value to steady-state temperature at the rate decided by the thermal time constant of the battery.

It is clear from the graph that all the charging strategies reach the final SOC level at the same time, but the operating temperature is different in all three cases. In further to comment on the uniformity in the evaluation under common

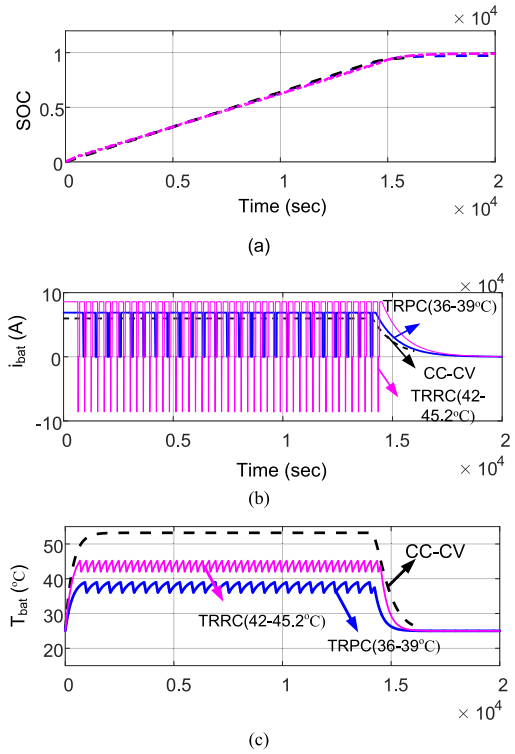

FIGURE 26. Variation in charging current and battery operating temperature for same SOC and charging time.

condition, Table-II is listed for different charging strategies with the condition of the same charging time and SOC level. Under such a situation, the magnitude of the injected current will be different, and accordingly operating temperature will also be different as shown in Fig. 26. For the same charging time (4.25hrs) and SOC level, the magnitude of the injected currents for the CC-CV, TRPC, and TRRC strategies are 2.3C/10 (= 5.98A), 2.65C/10 (= 6.89A) and 3.3C/10 (= 8.58A) respectively. Under this situation, battery operates at 53°C for CC-CV and for TRPC and TRRC it operates in the temperature band of 36-39°C and 42-45.2°C. As the operating temperature is different in all the three cases so accordingly expected life of the battery will be affected as explained in Fig.3 i.e. 24 months for TRPC and 10 months for CC-CV. Whereas, even though the life the battery for TRRC is comparatively lesser than TRPC but it results in better SOH as compared to TRPC has shown in Fig. 25, since in this charging strategy the battery is charged and discharged for each charging pulse. So, battery health deteriorates less in the case of the reflex charging strategy. Based on the above discussion it can be concluded that to ensure the same operating temperature as for TRPC/TRRC, CC-CV strategy requires injection of the current of lower magnitude. This will result in longer charging time with CC-CV. Hence it is verified that the TRPC strategy not only reduces the charging time to 60% as compared to normal charging i.e. 10 hours(C/10) but also improve the battery life and health.

VII. CONCLUSION

Present work demonstrates the comparative evaluation of unregulated and regulated charging strategies in order to find a suitable fast charging strategy for the valve regulated lead-acid batteries with improved life and health. A discrete electro-thermal model of a battery has been utilized to ensure temperature regulation and to determine the internal parameters of the battery. Evaluation is carried out between temperature unregulated charging strategy CC-CV and temperature regulated pulse (TRPC) and reflex (TRRC) charging strategy at the same time and SOC level. The operation of the temperature regulated pulse and reflex charging is divided into three sections 1, 2, and 3 based on the charging strategy and temperature reference. The unregulated zone is section-1, where the magnitude of charging current is not sufficient to exceed the upper limit of the band. Therefore, in this region constant current is injected into the battery. Temperature regulated zones are section 2 and 3 in this section the magnitude of charging current is such that the temperature reaches the maximum limit of that band, and pulse and reflex charging mechanism occurs. Section-2 is considered as an effective region for the fast charging of a valve regulated lead-acid battery. It has been verified that with the upward shift in the temperature reference the charge deposited in the battery increases. It is demonstrated that with temperature regulated pulse charging strategy, charging time is reduced to 60% as compared to conventional unregulated CC-CV (C/10) strategy. Further, the battery health is a significant concern which is considered during battery charging. It has been verified that battery health is improved through both TRPC and TRRC strategies as compared with CC-CV strategy with the same charging time and SOC level. It is demonstrated that the temperature regulated pulse charging strategy is suitable for fast charging of a VRLA battery with improved life and health.

REFERENCES

[1] C. Zhang, K. Li, and J. Deng, "Real-time estimation of battery internal temperature based on a simplified thermoelectric model," *J. Power Sources*, vol. 302, pp. 146–154, Jan. 2016.

[2] L. Zhang, H. Peng, Z. Ning, Z. Mu, and C. Sun, "Comparative research on RC equivalent circuit models for lithium-ion batteries of electric vehicles," *Appl. Sci.*, vol. 7, no. 10, p. 1002, Sep. 2017.

[3] C. C. Hua and M. Y. Lin, "A study of charging control of lead-acid battery for electric vehicles," in *Proc. IEEE ISIE*, vol. 1, Dec. 2000, pp. 135–140.

[4] T. Ikeya, N. Sawada, J.-I. Murakami, K. Kobayashi, M. Hattori, N. Murotani, S. Ujiie, K. Kajiyama, H. Nasu, H. Narisoko, Y. Tomaki, K. Adachi, Y. Mita, and K. Ishihara, "Multi-step constant-current charging method for an electric vehicle nickel/metal hydride battery with high-energy efficiency and long cycle life," *J. Power Sources*, vol. 105, no. 1, pp. 6–12, Mar. 2002.

[5] Y.-D. Lee and S.-Y. Park, "Rapid charging strategy in the constant voltage mode for a high power Li-ion battery," in *Proc. IEEE ECCE*, Sep. 2013, pp. 4725–4731.

[6] D. P. Reid and I. Glasa, "A new concept: Intermittent charging of lead acid batteries in telecommunication systems," in *Proc. IEEE INTELEC*, Nov. 1984, pp. 67–71.

[7] H. A. Catherino, F. F. Feres, and F. Trinidad, "Sulfation in lead-acid batteries," *J. Power Sources*, vol. 129, no. 1, pp-113-120, 2004.

[8] L.-R. Chen, N.-Y. Chu, C.-S. Wang, and R.-H. Liang, "Design of a reflex-based bidirectional converter with the energy recovery function," *IEEE Trans. Ind. Electron.*, vol. 55, no. 8, pp. 3022–3029, Aug. 2008.
[9] L. Song and J. W. Evans, "Electrochemical-thermal model of lithium polymer batteries," *J. Electrochem. Soc.*, vol. 147, no. 6, pp. 2086–2095, 2000.
[10] Z. M. Salameh, M. A. Casacca, and W. A. Lynch, "A mathematical model for lead-acid batteries," *IEEE Trans. Energy Convers.*, vol. 7, no. 1, pp. 93–98, Mar. 1992.
[11] M. Chen and G. A. Rincon-Mora, "Accurate electrical battery model capable of predicting runtime and I–V performance," *IEEE Trans. Energy Convers.*, vol. 21, no. 2, pp. 504–511, Jun. 2006.
[12] Y.-H. Liu, J.-H. Teng, and Y.-C. Lin, "Search for an optimal rapid charging pattern for Lithium–Ion batteries using ant colony system algorithm," *IEEE Trans. Ind. Electron.*, vol. 52, no. 5, pp. 1328–1336, Oct. 2005.
[13] L.-R. Chen, R. C. Hsu, and C.-S. Liu, "A design of a grey-predicted li-ion battery charge system," *IEEE Trans. Ind. Electron.*, vol. 55, no. 10, pp. 3692–3701, Oct. 2008.
[14] H. Surmann, "Genetic optimization of a fuzzy system for charging batteries," *IEEE Trans. Ind. Electron.*, vol. 43, no. 5, pp. 541–548, Oct. 1996.
[15] L. Xu, J. Wang, and Q. Chen, "Kalman filtering state of charge estimation for battery management system based on a stochastic fuzzy neural network battery model," *Energy Convers. Manage.*, vol. 53, no. 1, pp. 33–39, Jan. 2012.
[16] P. Keil and A. Jossen, "Charging protocols for lithium-ion batteries and their impact on cycle life—An experimental study with different 18650 high-power cells," *J. Energy Storage*, vol. 6, pp. 125–141, May 2016.
[17] T. T. Vo, X. Chen, W. Shen, and A. Kapoor, "New charging strategy for lithium-ion batteries based on the integration of Taguchi method and state of charge estimation," *J. Power Sources*, vol. 273, pp. 413–422, Jan. 2015.
[18] J. Jaguemont, L. Boulon, and Y. Dubé, "A comprehensive review of lithium-ion batteries used in hybrid and electric vehicles at cold temperatures," *Appl. Energy*, vol. 164, pp. 99–114, Feb. 2016.
[19] Y.-S. Lee and M.-W. Cheng, "Intelligent control battery equalization for series connected lithium-ion battery strings," *IEEE Trans. Ind. Electron.*, vol. 52, no. 5, pp. 1297–1307, Oct. 2005.
[20] L. H. Saw, Y. Ye, and A. A. O. Tay, "Electro-thermal characterization of lithium iron phosphate cell with equivalent circuit modeling," *Energy Convers. Manage.*, vol. 87, pp. 367–377, Nov. 2014.
[21] M. Alhanouti, M. Gießler, T. Blank, and F. Gauterin, "New electro-thermal battery pack model of an electric vehicle," *Energies*, vol. 9, no. 7, p. 563, Jul. 2016.
[22] L. Song, L. Li, Z. Xiao, J. Zhang, Z. Cao, Q. Zhou, C. Hu, and J. Liu, "Estimation of temperature distribution of $LiFePO_4$ lithium ion battery during charge–discharge process," *Ionics*, vol. 22, no. 9, pp. 1517–1525, Sep. 2016.
[23] X. Hu, S. Li, H. Peng, and F. Sun, "Charging time and loss optimization for LiNMC and $LiFePO_4$ batteries based on equivalent circuit models," *J. Power Sources*, vol. 239, pp. 449–457, Oct. 2013.
[24] D. Anseán, M. González, J. C. Viera, V. M. García, C. Blanco, and M. Valledor, "Fast charging technique for high power lithium iron phosphate batteries: A cycle life analysis," *J. Power Sources*, vol. 239, pp. 9–15, Oct. 2013.
[25] L. R. Chen, "Design of duty-varied voltage pulse charger for improving Li-ion battery-charging response," *IEEE Trans. Ind. Electron.*, vol. 56, no. 2, pp. 480–487, Feb. 2009.
[26] L.-R. Chen, S.-L. Wu, D.-T. Shieh, and T.-R. Chen, "Sinusoidal-ripple-current charging strategy and optimal charging frequency study for li-ion batteries," *IEEE Trans. Ind. Electron.*, vol. 60, no. 1, pp. 88–97, Jan. 2013.
[27] L. Patnaik, A. V. J. S. Praneeth, and S. S. Williamson, "A closed-loop constant-temperature constant-voltage charging technique to reduce charge time of lithium-ion batteries," *IEEE Trans. Ind. Electron.*, vol. 66, no. 2, pp. 1059–1067, Feb. 2019.
[28] K. Liu, K. Li, and C. Zhang, "Constrained generalized predictive control of battery charging process based on a coupled thermoelectric model," *J. Power Sources*, vol. 347, pp. 145–158, Apr. 2017.
[29] C. Zhang, J. Jiang, Y. Gao, W. Zhang, Q. Liu, and X. Hu, "Charging optimization in lithium-ion batteries based on temperature rise and charge time," *Appl. Energy*, vol. 194, pp. 569–577, May 2017.
[30] A. Abdollahi, X. Han, G. V. Avvari, N. Raghunathan, B. Balasingam, K. R. Pattipati, and Y. Bar-Shalom, "Optimal battery charging, part I: Minimizing time-to-charge, energy loss, and temperature rise for OCV-resistance battery model," *J. Power Sources*, vol. 303, pp. 388–398, Jan. 2016.
[31] Q. Ouyang, Z. Wang, K. Liu, G. Xu, and Y. Li, "Optimal charging control for lithium-ion battery packs: A distributed average tracking approach," *IEEE Trans. Ind. Informat.*, vol. 16, no. 5, pp. 3430–3438, May 2020.
[32] H. E. Perez, X. Hu, S. Dey, and S. J. Moura, "Optimal charging of Li-ion batteries with coupled electro-thermal-aging dynamics," *IEEE Trans. Veh. Technol.*, vol. 66, no. 9, pp. 7761–7770, Sep. 2017.
[33] X. Hu, Y. Zheng, X. Lin, and Y. Xie, "Optimal multistage charging of NCA/Graphite lithium-ion batteries based on electrothermal-aging dynamics," *IEEE Trans. Transport. Electrific.*, vol. 6, no. 2, pp. 427–438, Jun. 2020, doi: 10.1109/TTE.2020.2977092.
[34] K. Liu, X. Hu, Z. Yang, Y. Xie, and S. Feng, "Lithium-ion battery charging management considering economic costs of electrical energy loss and battery degradation," *Energy Convers. Manage.*, vol. 195, pp. 167–179, Sep. 2019.
[35] X. Lin, H. E. Perez, J. B. Siegel, A. G. Stefanopoulou, Y. Li, R. D. Anderson, Y. Ding, and M. P. Castanier, "Online parameterization of lumped thermal dynamics in cylindrical lithium ion batteries for core temperature estimation and health monitoring," *IEEE Trans. Control Syst. Technol.*, vol. 21, no. 5, pp. 1745–1755, Sep. 2013.
[36] D. Zhang, S. Dey, H. E. Perez, and S. J. Moura, "Real-time capacity estimation of lithium-ion batteries utilizing thermal dynamics," *IEEE Trans. Control Syst. Technol.*, vol. 28, no. 3, pp. 992–1000, May 2020.
[37] M. Coleman, C. Kwan Lee, C. Zhu, and W. G. Hurley, "State-of-charge determination from EMF voltage estimation: Using impedance, terminal voltage, and current for lead-acid and lithium-ion batteries," *IEEE Trans. Ind. Electron.*, vol. 54, no. 5, pp. 2550–2557, Oct. 2007.
[38] N. H. F. Ismail, S. F. Toha, N. A. M. Azubir, N. H. M. Ishak, M. K. Hassan, and B. S. K. S. M. Ibrahim, "Simplified heat generation model for lithium ion battery used in electric vehicle," in *Proc. IOP Conf. Ser., Mater. Sci. Engg.*, vol. 53, no. 1, 2013, Art. no. 012014.
[39] *12V, 26Ah, Sealed Maintenance Free VRLA Batteries*. Accessed: 2019. [Online]. Available: http://aclbaterias.es/wp-content/uploads/2019/01/CEIL_Power-Safe-Brochure-OK1.pdf
[40] EXIDE Technologies Gmbh, Büdingen, Germany. *Handbook for Stationary Lead-Acid Batteries*. Accessed: Feb. 2012. [Online]. Available: https://docplayer.net/23551953-Handbook-for-stationary-lead-acid-batteries-part-1-basics-design-operation-modes-and applications.html
[41] M. R. Moore, F. L. Tarantino, F. J. Chiacchio, and J. R. Resurreccion, "Real-time expected life on VRLA products—A manufacturers' perspective," in *Proc. 17th Int. Telecommun. Energy Conf. (INTELEC)*, The Hague, The Netherlands, 1995, pp. 65–69.
[42] J. Wang, P. Liu, J. Hicks-Garner, E. Sherman, S. Soukiazian, M. Verbrugge, H. Tataria, J. Musser, and P. Finamore, "Cycle-life model for graphite-LiFePO4 cells," *J. Power Sources*, vol. 196, no. 8, pp. 3942–3948, Apr. 2011.
[43] B.-Y. Chen and Y.-S. Lai, "New digital-controlled technique for battery charger with constant current and voltage control without current feedback," *IEEE Trans. Ind. Electron.*, vol. 59, no. 3, pp. 1545–1553, Mar. 2012.
[44] K. K. Yeung, X. Zhang, S. C. T. Kwok, F. Ciucci, and M. M. F. Yuen, "Enhanced cycle life of lead-acid battery using graphene as a sulfation suppression additive in negative active material," *RSC Adv.*, vol. 5, no. 87, pp. 71314–71321, 2015.
[45] Q. Long, G. Ma, Q. Xu, C. Ma, J. Nan, A. Li, and H. Chen, "Improving the cycle life of lead-acid batteries using three-dimensional reduced graphene oxide under the high-rate partial-state-of-charge condition," *J. Power Sources*, vol. 343, pp. 188–196, Mar. 2017.
[46] M. Bhatt, W. G. Hurley, and W. H. Wolfle, "A new approach to intermittent charging of valve-regulated lead-acid batteries in standby applications," *IEEE Trans. Ind. Electron.*, vol. 52, no. 5, pp. 1337–1342, Oct. 2005.
[47] C. Praisuwanna and S. Khomfoi, "A pulse frequency technique for a quick charger," in *Proc. IEEE ECTI-CON*, May 2013, pp. 1–6.
[48] Z. Jiang and R. A. Dougal, "Synergetic control of power converters for pulse current charging of advanced batteries from a fuel cell power source," *IEEE Trans. Power Electron.*, vol. 19, no. 4, pp. 1140–1150, Jul. 2004.
[49] Y. C. Hsieh, C. S. Moo, C. K. Wu, and J. C. Cheng, "A non-dissipative reflex charging circuit," in *Proc. IEEE INTELEC*, Jun. 2003, pp. 679–683.
[50] A. Bakker and J. H. Huijsing, "Micropower CMOS temperature sensor with digital output," *IEEE J. Solid-State Circuits*, vol. 31, no. 7, pp. 933–937, Jul. 1996.
[51] L. R. Chen, C. S. Wang, W. R. Yang, and N. Y. Chu, "A novel bidirectional converter with the reflex charging function," in *Proc. IEEE Int. Conf. Ind. Technol.*, Chengdu, China, Apr. 2008, pp. 1–6.

SANDHYA LAVETY received the B.E. degree in electrical engineering from the University of Rajasthan, India, in 2010, and the M.Tech. degree in electrical engineering from IEC, UPTU, India, in 2014. She is currently pursuing the Ph.D. degree with the Visvesvaraya National Institute of Technology, Nagpur, India.

Her research interest includes power electronics systems for electric vehicle charging. She received the MEITY Fellowship for the Ph.D. degree and the Women Innovator Award from MSME, in 2019.

RITESH KUMAR KESHRI (Senior Member, IEEE) received the B.Sc.Engg. and M.Tech. degrees in electrical engineering from the National Institute of Technology, Jamshedpur, India, in 2003 and 2007, respectively, and the Ph.D. degree from the University of Padova, Italy, in 2014.

Since 2015, he has been with the Department of Electrical Engineering, Visvesvaraya National Institute of Technology, Nagpur, India, as an Assistant Professor. From January 2008 to December 2008, he was with the University of Padova, as a Young Researcher, where he was an Erasmus Mundus Doctoral Research Scholar, from August 2010 to July 2013. His research interests include application of power electronics, drives for electric vehicle sub-systems, and charging infrastructure.

Dr. Keshri was on the Technical Committee on Transportation Electrification with the IEEE IES. He was one of the organizers of special sessions and technical tracks from IECON 2013 to 2019. He received the Young Researcher Fellowship from the Ministry of University, Italy, in 2008, the Erasmus Mundus Doctoral Research Fellowship under Willpower from the European Union, in 2010, the First Prize from the Class Three Formula Electric and Hybrid, Turin, Italy, in 2011, the Student Team Leader of Battery Ultra Capacitor System for Mobility (BUS4M) for the Best Project and Business Plan, the 2016 Best Paper Award from the IEEE TRANSACTION ON INDUSTRIAL ELECTRONICS, and the Visvesvaraya Young Faculty Research Award in 2017. He serves as the Chair for the IEEE IES.

MADHURI A. CHAUDHARI (Senior Member, IEEE) was born in India, in January 1968. She received the B.E. degree in electrical engineering from Amaravati University, Amaravati, India, the M.Tech. degree in electrical engineering from the Visvesvaraya Regional College of Engineering, Nagpur University, Nagpur, India, and the Ph.D. degree in electrical engineering from the Visvesvaraya National Institute of Technology, Nagpur, in June 2007. She is currently a Professor and the Head of the Department of Electrical Engineering, Visvesvaraya National Institute of Technology. Her research interests include power electronics, flexible ac transmission systems, grid connected converters, multilevel inverters, drives and their control techniques, and so on. She is a Fellow of the Institution of Engineers, a Life Member of ISTE, and a member of the Indian Society of Industrial and Applied Mathematics.